REGULAR PAPER

Accurate measurement of elasticity of the radial artery wall considering changes in cross-sectional shape of artery caused by pushing pressure applied by ultrasound probe

Japanese Journal of Applied Physics **61**, SG1042 (2022) **REGULAR PAPER**
https://doi.org/**10.35848/1347-4065/ac4e4a**

Accurate measurement of elasticity of the radial artery wall considering changes in cross-sectional shape of artery caused by pushing pressure applied by ultrasound probe

Yuto Shoji[1], Shohei Mori[2], Mototaka Arakawa[1,2*], Shigeo Ohba[2], Kazuto Kobayashi[3], and Hiroshi Kanai[2,1]

[1]*Graduated School of Biomedical Engineering, Tohoku University, Sendai 980-8579, Japan*
[2]*Graduated School of Engineering, Tohoku University, Sendai 987-8579, Japan*
[3]*Honda Electronics Co. Ltd., Toyohashi 441-3193, Japan*

[*]E-mail: arakawa@ecei.tohoku.ac.jp

Received November 2, 2021; revised January 6, 2022; accepted January 24, 2022; published online May 27, 2022

For the early diagnosis of atherosclerosis, our group developed an ultrasound probe that can simultaneously measure blood pressure and vessel diameter at the same position. However, because the developed probe requires the blood vessel to be deformed by pushing to measure the blood pressure, it affects the estimation of the vessel's elastic modulus. In the present study, we derived a series of equations to estimate the elastic modulus of a blood vessel considering the pushing pressure applied by the ultrasound probe and the resultant deformation of the blood vessel. The validity of the proposed method was verified by numerical calculations, and then the method was applied to in vivo measurements. The proposed method resulted in fewer variations in the elastic modulus estimates with different pushing pressures compared with the conventional method.

1. Introduction

Cardiovascular diseases, including ischemic heart disease and stroke, are the leading cause of death worldwide.[1)] The main cause of cardiovascular diseases is atherosclerosis. It has been clinically diagnosed using several techniques, including intravascular ultrasound[2)] and X-ray imaging.[3)] However, these techniques are not noninvasive. Alternatively, pulse wave velocity,[4)] ankle-brachial index,[5)] cardio-ankle-brachial index,[6)] stiffness parameter,[7)] and elasticity[8)] have been proposed as noninvasive diagnostic methods for atherosclerosis. However, these methods can only be applied to diagnose advanced-stage atherosclerosis, which is irreversible. At the early stage of atherosclerosis, vascular endothelial dysfunction occurs, and it is possible to be completely cured of atherosclerosis by medication and/or lifestyle improvement.[9)] Therefore, early diagnosis is important.

Plethysmography[10,11)] and the flow-mediated dilatation (FMD) test[12–14)] are the main clinical methods used to evaluate vascular endothelial function. In plethysmography, vascular endothelial function is evaluated by measuring the changes in blood flow caused by injecting a vasodilator such as acetylcholine into the blood vessel. In the FMD test, vascular endothelial function is evaluated by ultrasonically measuring the dilatation ratio %FMD of the arterial diameter after releasing the avascularization to that at rest. As the FMD test is simple and non-invasive, it has been widely adopted by, for example, the Framingham Heart Study, and the clinical data on the relationship between %FMD and various risk factors have been accumulated worldwide.[15,16)] However, the distance resolution of the ultrasound measurement is 0.15 mm with a typical 10 MHz ultrasound probe. For healthy subjects, the %FMD is about 6% or more, which corresponds to only 0.24–0.30 mm when the diameter of the vessel is 4–5 mm. Accurate evaluation of the %FMD is difficult.

Furthermore, a change in the diameter of an artery due to endothelial function is caused by changes in the mechanical properties of the arterial wall; however, these changes cannot be used to directly evaluate endothelial function. A method for evaluating endothelial function by analyzing the pulse wave waveforms in the radial artery has also been studied,[17,18)] referring to a method to estimate stiffness parameters from the pulse wave analysis.[19)] However, this method also indirectly evaluates endothelial function because it evaluates the features of the pulse wave waveform.

In the FMD response, an increase in blood flow produces the vasodilator nitric oxide (NO), which decreases the elasticity of the arterial wall and increases the arterial diameter.[20,21)] If the decrease in the vascular elasticity caused by NO can be noninvasively measured, direct evaluation of vascular endothelial function can be achieved.

Our group has focused on ultrasonic measurement of the relationship between the changes in the strain of the vessel wall and the blood pressure during one heartbeat to estimate the changes in the elastic and viscous moduli during FMD.[22–25)] However, accurate viscoelasticity measurements were difficult because the measurement positions of the vessel diameter for the calculation of the strain and the pressure waveform were different.

Sakai et al. proposed a method for measuring the blood pressure waveform and the strain of the vessel wall at the same position by a correction determined from the delay between the pressure waveforms measured by two pressure sensors, where the ultrasound probe for the strain measurement was placed at the center of the two pressure sensors.[26,27)] However, it was difficult to accurately determine the delay between the two pressure waveforms because it depends on the instantaneous pressure of the pressure waveforms.

Therefore, our group has developed an ultrasound probe that can simultaneously measure the blood pressure waveform and the change in the vascular diameter at the same position.[28,29)] Furthermore, we have proposed a method for measuring viscoelasticity over time by calibrating the blood pressure waveform at rest in advance,[30)] and have measured the changes in viscoelasticity at the radial artery during the FMD.[31)] However, the voltage output from the center element of the probe depends on the pressure applied by the ultrasound probe during the measurement.

Therefore, we introduced the pulse transit time method to determine the blood pressure, as it is not affected by the

absolute value of the acquired voltage output, and a stable blood pressure measurement was achieved with it during the FMD.[32] However, the changes in the cross-sectional shape of the vessel caused by the pushing pressure applied by the ultrasound probe still had an effect on the viscoelasticity estimation.

Therefore, to consider the effect of the deformation of the arterial cross-section from a circular to an elliptical shape caused by the pushing of the ultrasound probe, we derived a series of equations to estimate the elastic modulus[33] based on the derivation of the equations for estimating the elastic modulus of the artery with a circular shape proposed by Hasegawa et al.[34]

In the present study, we applied the derived equations to estimate the elastic modulus using in vivo measurements. The elastic modulus was estimated by measuring the changes in the vessel diameter and blood pressure in the radial artery during one heartbeat when different pushing pressures were applied by the ultrasound probe. From the experiments conducted with a healthy subject, it was confirmed that the estimates of the elastic modulus obtained using the derived equations were similar regardless of the change in the cross-sectional shape of the vessel caused by the pushing pressure applied by the ultrasound probe.

2. Experimental methods

The pushing by the probe to measure the blood pressure using the center element of the developed ultrasound probe causes deformation of the cross-sectional shape of the blood vessel.[28,29] By assuming that the cross-sectional shape of the vessel after deformation is elliptical, a series of equations that can be used to estimate the elastic modulus under the pushing by the ultrasound probe was derived. In general, the relationships among the elastic modulus E, incremental stress $\Delta\sigma$, and incremental strain $\Delta\varepsilon$ of viscoelastic material in a cylindrical coordinate system are given by:[35]

$$\Delta\varepsilon_r = \frac{\Delta\sigma_r}{E_r} - \frac{\nu\Delta\sigma_\theta}{E_\theta} - \frac{\nu\Delta\sigma_z}{E_z}, \tag{1}$$

$$\Delta\varepsilon_\theta = -\frac{\nu\Delta\sigma_r}{E_r} + \frac{\Delta\sigma_\theta}{E_\theta} - \frac{\nu\Delta\sigma_z}{E_z}, \tag{2}$$

$$\Delta\varepsilon_z = -\frac{\nu\Delta\sigma_r}{E_r} - \frac{\nu\Delta\sigma_\theta}{E_\theta} + \frac{\Delta\sigma_z}{E_z}, \tag{3}$$

where r, θ, and z are the direction of the vessel wall, the circumferential direction of the vessel wall, and the axial direction of the vessel, respectively, as shown in Fig. 1, and ν is Poisson's ratio. As the vessel is strongly constrained in the axial direction in vivo, the incremental axial strain $\Delta\sigma_z$ can be ignored. In the present study, the vessel wall was assumed to be isotropic, that is, $E = E_r = E_\theta = E_z$. Moreover, assuming that the strain caused by the heartbeat is incompressible ($\nu = 1/2$), Eqs. (1)–(3) can be rewritten as

$$\Delta\varepsilon_r = \frac{\Delta\sigma_r}{E} - \frac{\Delta\sigma_\theta}{2E} - \frac{\Delta\sigma_z}{2E}, \tag{4}$$

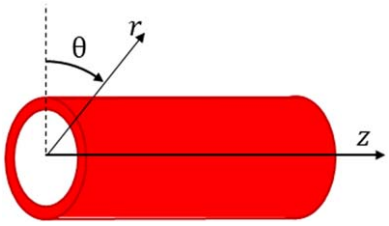

Fig. 1. (Color online) Schematic of the cylindrical coordinate system in a blood vessel.

$$\Delta\varepsilon_\theta = -\frac{\Delta\sigma_r}{2E} + \frac{\Delta\sigma_\theta}{E} - \frac{\Delta\sigma_z}{2E}, \tag{5}$$

$$0 = -\frac{\Delta\sigma_r}{2E} - \frac{\Delta\sigma_\theta}{2E} + \frac{\Delta\sigma_z}{E}. \tag{6}$$

From Eq. (6),

$$\Delta\sigma_z = \frac{1}{2}(\Delta\sigma_r + \Delta\sigma_\theta). \tag{7}$$

By rearranging Eqs. (4) and (5) for E and substituting Eq. (7) into them, we obtain

$$E = \frac{3}{4\Delta\varepsilon_r}(\Delta\sigma_r - \Delta\sigma_\theta), \tag{8}$$

$$E = \frac{3}{4\Delta\varepsilon_\theta}(\Delta\sigma_\theta - \Delta\sigma_r). \tag{9}$$

Thus, the elastic modulus E can be estimated from $\Delta\varepsilon_r$ or $\Delta\varepsilon_\theta$, $\Delta\sigma_r$, and $\Delta\sigma_\theta$.

Let us now consider the case in which the radial artery is deformed by a change in internal pressure p_1 due to a heartbeat under the pushing pressure p_3 applied by the ultrasound probe. The cross-sectional shape of the artery is assumed to deform from a circular to an elliptical shape with a long radius b and a short radius a because of the uniform pressure p_3 acting on the upper surface of the artery in the y direction, as shown in Fig. 2(a). Figure 2(b) shows a magnified view of a small region of the vessel, where p_2 is the atmospheric pressure, T is the tension acting along the circumferential direction ϕ of the wall, ρ is the curvature radius of the region of the vessel, and h is the thickness of the vessel wall. The intravascular pressure p_1 is assumed to be uniformly applied regardless of ϕ. The thickness h of the vessel wall was assumed to be constant during the transformation of the cross-sectional shape of the vessel from a circle to an ellipse. The tension T acting along the circumferential direction of the wall is not uniform because the cross-sectional shape of the vessel is an ellipse, and it changes even for the region.

From the balance among the forces acting on the region in the x direction and the y direction, Eqs. (10) and (11) are obtained as follows:

$$T\sin(\phi - d\phi) - (T + dT)\sin(\phi + d\phi) + p_1 dL_1\cos\phi - p_2 dL_2\cos\phi = 0, \tag{10}$$

$$-T\cos(\phi - d\phi) + (T + dT)\cos(\phi + d\phi) + p_1 dL_1\sin\phi - p_2 dL_2\sin\phi - p_3 dL_2\sin\phi = 0, \tag{11}$$

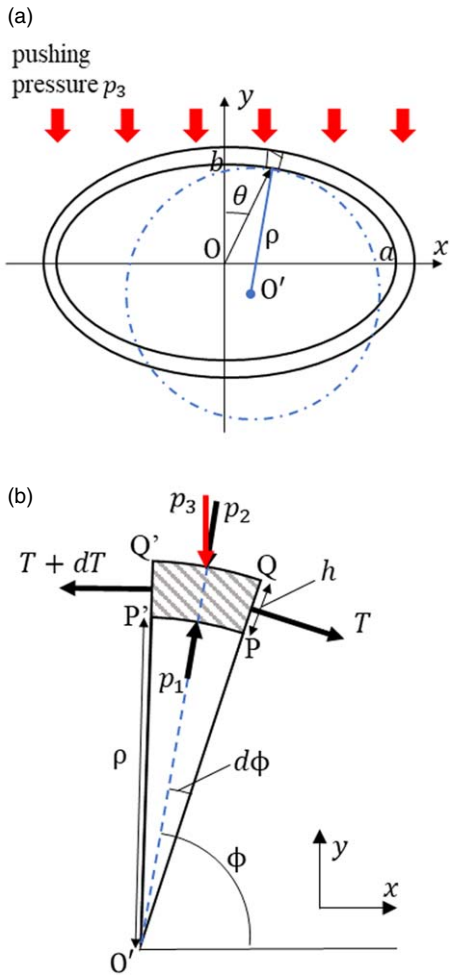

Fig. 2. (Color online) Cross-section of the blood vessel deformed into an ellipse by a uniform pressure. (a) Schematic of the cross-section of a blood vessel and (b) magnified view of the small portion of the blood vessel wall.

where dL_1 and dL_2 are the lengths of PP′ and QQ′, respectively, and are given by

$$dL_1 = 2\rho d\phi, \tag{12}$$

$$dL_2 = 2(\rho + h)d\phi. \tag{13}$$

By substituting Eqs. (12) and (13) into Eqs. (10) and (11), we obtain

$$T\sin(\phi - d\phi) - (T + dT)\sin(\phi + d\phi) + 2p_1\rho d\phi\cos\phi - 2p_2(\rho + h)d\phi\cos\phi = 0, \tag{14}$$

$$-T\cos(\phi - d\phi) + (T + dT)\cos(\phi + d\phi) + 2p_1\rho d\phi\sin\phi - 2p_2(\rho + h)d\phi\sin\phi - 2p_3(\rho + h)d\phi\sin\phi = 0. \tag{15}$$

By expanding these equations using the additive theorem of trigonometric functions and the approximations $\sin d\phi = d\phi$ and $\cos d\phi = 1 - d\phi^2/2$, where $d\phi$ is assumed to be minute, we obtain

$$-dT\left\{\sin\phi\left(1 - \frac{d\phi^2}{2}\right) - d\phi\cos\phi\right\} - 2d\phi\cos\phi\{T - p_1\rho - p_2(\rho + h)\} = 0, \tag{16}$$

$$dT\left\{\cos\phi\left(1 + \frac{d\phi^2}{2}\right) - d\phi\sin\phi\right\} - 2d\phi\sin\phi\{T + p_1\rho - (p_2 + p_3)(\rho + h)\} = 0. \tag{17}$$

By approximating these equations to first-order equations in terms of $d\phi$ and dT, and rearranging them in terms of dT, we obtain

$$dT = -\frac{2d\phi}{\tan\phi}\{T - p_1\rho - p_2(\rho + h)\}, \tag{18}$$

$$dT = 2d\phi\tan\phi\{T + p_1\rho - (p_2 - p_3)(\rho + h)\}. \tag{19}$$

Eliminating dT by substituting Eq. (19) into Eq. (18) and rearranging in terms of T gives

$$T = \rho\left(p_1 - p_2 - \frac{\tan^2\phi}{1 + \tan^2\phi}p_3\right) - h\left(p_2 + \frac{\tan^2\phi}{1 + \tan^2\phi}p_3\right). \tag{20}$$

Assuming that the circumferential stress is uniform along the through-wall direction, the circumferential stress σ_θ is obtained by dividing the tension T of Eq. (20) by the wall thickness h:

$$\sigma_\theta = \frac{\rho}{h}\left(p_1 - p_2 - \frac{\tan^2\phi}{1 + \tan^2\phi}p_3\right) - \left(p_2 + \frac{\tan^2\phi}{1 + \tan^2\phi}p_3\right). \tag{21}$$

On the other hand, because the through-wall stress σ_r equals $-p_1$ at PP′ in the inner wall and it equals the sum of $-p_2$ and the through-wall component of $-p_3$ at QQ′ in the outer wall, assuming the through-wall stress σ_r is distributed uniformly in the direction of the through-wall, then σ_r is given by the average values of p_1 and the sum of p_2 and $p_3\cos\phi$ considering the balance of forces:

$$\sigma_r = -\frac{1}{2}(p_1 + p_2 + p_3\cos\phi). \tag{22}$$

By rewriting Eqs. (21) and (22) using a, b, and θ shown in Fig. 2(a) instead of the curvature radius ρ, $\cos\phi$, and $\tan\phi$, we obtain

$$\sigma_\theta = \frac{1}{abh}\left(\frac{a^2 + b^2\tan^2\theta}{1 + \tan^2\theta}\right)^{\frac{3}{2}}\left(p_1 - p_2 - \frac{a^2}{a^2 + b^2\tan^2\theta}p_3\right) - \left(p_2 + \frac{a^2}{a^2 + b^2\tan^2\theta}p_3\right), \tag{23}$$

$$\sigma_r = -\frac{1}{2}\left(p_1 + p_2 + \frac{b\tan\theta}{\sqrt{a^2\tan^2\theta + b^2}}p_3\right). \tag{24}$$

Thus, σ_θ and σ_r, which are required for estimating the elastic modulus E, are calculated from a, b, the angle θ of the region from the y axis, p_1, p_2, and the pushing pressure p_3 applied by the ultrasound probe.

By subtracting the stresses σ_θ and σ_r at diastole from at systole, the incremental stresses $\Delta\sigma_\theta$ and $\Delta\sigma_r$ can be obtained. The elastic modulus E is estimated by substituting $\Delta\sigma_\theta$ and $\Delta\sigma_r$, and the circumferential strain $\Delta\varepsilon_\theta$ measured by ultrasound into Eq. (9).

The process of estimating the elastic modulus in the actual measurements is now described. To estimate the elastic modulus, the value of the circumferential strain $\Delta\varepsilon_\theta$ is required. However, $\Delta\varepsilon_\theta$ cannot be measured directly. Using the change in the short radius b of the vessel obtained by applying the phased-tracking method[36] to the RF signal of the beam passing through the center of the vessel, as in the conventional method,[30–32] $\Delta\varepsilon_\theta$ can be obtained as the ratio of the change in circumference to the original circumference:

$$\Delta\varepsilon_\theta = \frac{2\pi b_{\mathrm{sys}} - 2\pi b_{\mathrm{dias}}}{2\pi b_{\mathrm{dias}}} = \frac{b_{\mathrm{sys}} - b_{\mathrm{dias}}}{b_{\mathrm{dias}}}, \tag{25}$$

where b_{sys} and b_{dias} denote the short radii at systole and diastole, respectively, and the small region is a part of a circle with radii b_{sys} or b_{dias}.

When the strain $\Delta\varepsilon_\theta$ is defined along the beam passing through the center of the vessel ($\theta = 0°$), the stress should also be calculated at $\theta = 0°$, and Eqs. (23) and (24) are given by

$$\sigma_\theta = \frac{a^2}{bh}(p_1 - p_2 - p_3) - (p_2 + p_3), \tag{26}$$

$$\sigma_r = -\frac{1}{2}(p_1 + p_2 + p_3). \tag{27}$$

Therefore, the circumferential stress σ_θ and through-wall stress σ_r are determined from a, b, h, p_1, p_2, and p_3, each of which is measured as follows.

Figure 3(a) shows the B-mode image of the radial artery of a healthy subject. Figure 3(b) shows the normalized enveloped amplitude of the RF signals along the beam passing through the center of the vessel, as shown by the white line in Figs. 3(a)–3(c) shows the normalized enveloped amplitude of the RF signals along the red line in Fig. 3(a). From these figures, a and b were determined as 2.1 mm and 1.09 mm, respectively.

The change in b, $b_{\mathrm{sys}} - b_{\mathrm{dias}}$, of Eq. (25) was measured by applying the phased-tracking method[36] to the RF signal along the white line in Fig. 3(a). p_1 was measured by the center element of the developed ultrasound probe[28,29] with a center frequency of 7.5 MHz. The atmospheric pressure p_2 was assumed to be 1013.25 hPa in the present study. p_3 was measured by the pressure sensors separately attached to the ultrasonic probe, as described below in Fig. 4.

It is difficult to accurately measure the wall thickness h of the radial artery in vivo by ultrasound at 7.5 MHz owing to the lack of distance resolution. Therefore, in the present study, the wall thickness of the subject's radial artery was separately measured in advance using another ultrasound probe with a center frequency of 40 MHz, and $h = 0.235$ mm was used for the subject.

3. Experiments

3.1. Validation of the proposed equations by numerical calculations

We assumed that the pushing pressure p_3 was a constant during one heartbeat because the ultrasound probe was fixed for the measurement. On the other hand, the shape of the blood vessel changes between systole and diastole, and the stress σ_θ of Eq. (26), which includes a and b, is affected at $\theta = 0°$. In the present study, therefore, the derived equations for the estimation of elasticity during one heartbeat were confirmed by the following numerical calculations using the actual measured values of the intravascular pressure $p_1 = 106$ mmHg, long radius $a_{\mathrm{sys}} = 1.1$ mm, and short radius $b_{\mathrm{sys}} = 0.81$ mm of the radial artery in systole, and $p_1 = 55$ mmHg, $a_{\mathrm{dias}} = 1.1$ mm, and $b_{\mathrm{dias}} = 0.71$ mm in diastole. By assuming that the pressure p_3 was greater than p_1 in diastole because the vessel was deformed by the ultrasound probe, $p_3 = 70$ mmHg was employed. These values were substituted into Eq. (26).

First, to examine the relationship between the circumferential stress σ_θ and the position x on the arterial cross-section, σ_θ at systole and diastole, and the incremental stress $\Delta\sigma_\theta$ from diastole to systole were obtained for various values of θ from 0° to 180° using Eq. (26). Next, to examine the relationship between the circumferential stress σ_θ and the vessel shape, $\Delta\sigma_\theta$ from diastole to systole was obtained for various aspect

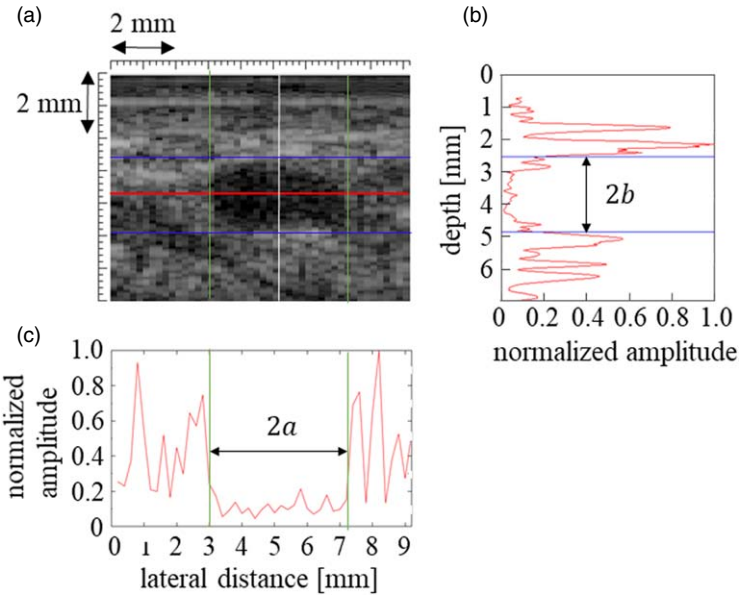

Fig. 3. (Color online) Calculation of the short and long radius of the vessel. (a) B-mode image of the radial artery, (b) normalized enveloped amplitude at the beam through the center of the vascular lumen, and (c) normalized enveloped amplitude at the depth of the center of the vascular lumen.

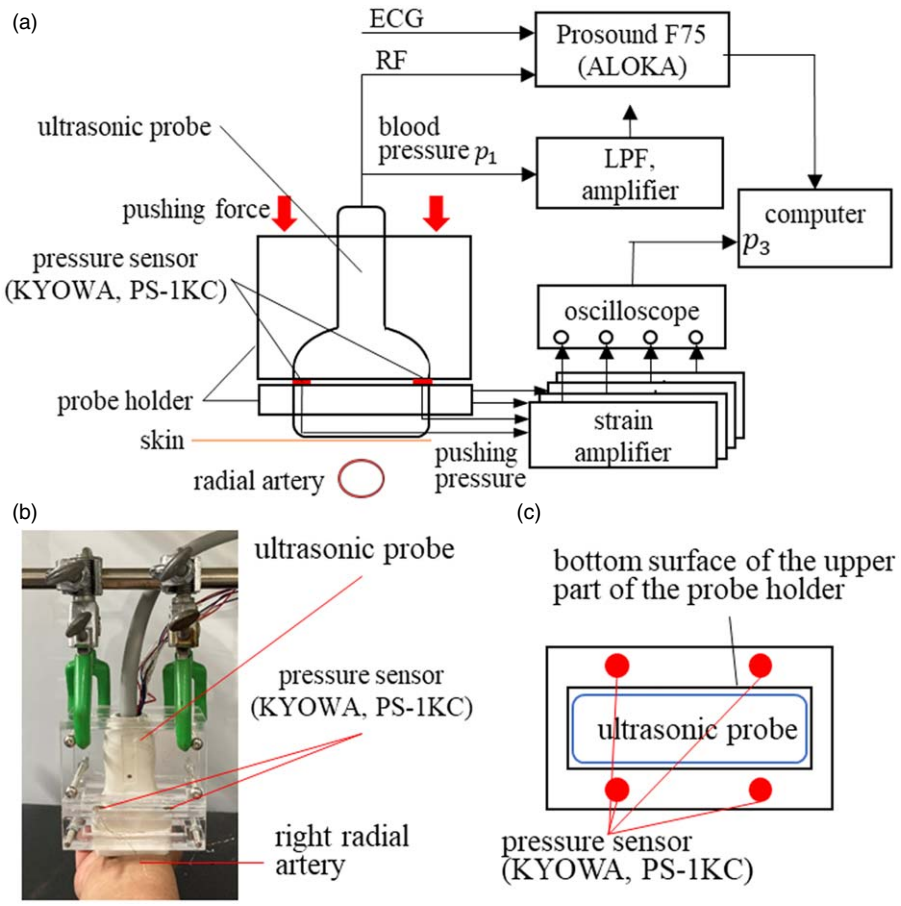

Fig. 4. (Color online) Schematic of the entire experimental system. (a) Block diagram, (b) photograph around the ultrasonic probe, and (c) arrangement of the pressure sensors.

ratios a/b of the vessel shape from 1 to 3. Finally, to examine the relationship between σ_θ and the pushing pressure p_3, $\Delta\sigma_\theta$ from diastole to systole was obtained for various pressure values p_3 from 0 to 150 mmHg using Eq. (26), with $\theta = 0°$.

3.2. In vivo experiment

Figure 4(a) shows a schematic of the entire experimental system, and Fig. 4(b) shows a photograph of the ultrasound probe. The long radius a of the vessel, the short radius b of the vessel, and the blood pressure p_1 were measured in the right radial artery using the developed ultrasound probe.[28,29]

The output from the piezoelectric element at the center of the ultrasound probe was passed through an amplifier with an amplification factor of 40 dB and a low-pass filter with a cutoff frequency of 30 Hz, and the blood pressure waveform was obtained by integrating the waveform. The measurement position was set such that the center of the probe was just above the radial artery while viewing the B-mode image. As the measured blood pressure waveform was output as a voltage, the absolute value of the blood pressure at systole and diastole measured by a sphygmomanometer and the absolute value of the waveform were calibrated by the pulse transit time method.[32] In the ultrasound measurement, the center frequency, sampling frequency, and frame rate were set to 7.5 MHz, 40 MHz, and 252 Hz, respectively. The long and short radii of vessels a and b were measured at systole and diastole, respectively. Electrocardiograms were also obtained.

The pushing pressure p_3 applied to the radial artery by the ultrasound probe was measured using four pressure sensors (Kyowa, PS-1KC). A probe holder consisting of the upper and lower parts that enclosed the ultrasound probe was fabricated, and four pressure sensors were placed between the two parts, as shown in Fig. 4(c). The ultrasound probe was fixed to the lower part of the probe holder, and the upper part could freely move up and down. From the force applied to the upper part of the probe holder, the pressure p_3 applied to the ultrasound probe was measured by an oscilloscope via strain amplifiers. p_3 was obtained by the sum p_{sum} of the forces applied to the four pressure sensors multiplied by the contact area S_{sensors} of the pressure sensors and divided by the contact area S_{probe} of the ultrasonic probe attached to the skin as follows:

$$p_3 = \frac{p_{\mathrm{sum}} \cdot S_{\mathrm{sensors}}}{S_{\mathrm{probe}}}, \tag{28}$$

where $S_{\mathrm{sensors}} = 36\pi \times 10^{-6}\,\mathrm{m}^2$ and $S_{\mathrm{probe}} = 1.53 \times 10^{-4}\,\mathrm{m}^2$ in the present study.

A healthy male subject in his early twenties was measured in a sitting position at rest. The subject was asked to avoid eating for three hours before the measurement and to rest for 30 min before the measurement to eliminate the effects of eating and exercise on blood pressure and the elastic modulus of the blood vessel, and to approach the condition in the FMD test. We obtained the approval of the ethics committee of our university and informed consent from the subject before the measurements. The blood pressure waveform and the blood vessel diameter were measured under three different conditions of various pushing pressures of the

ultrasound probe while the subject was at rest. Data were acquired for four seconds per measurement.

The proposed method was applied to the estimation of the elastic modulus of a blood vessel after three consecutive heartbeats using the measured vessel shape, blood pressure, and pushing pressure, and the results were compared with those obtained with our previous conventional method.[30–32)]

4. Result and discussion

4.1. Results of the numerical simulations

Figure 5 shows the calculated results of the circumferential stress σ_θ for systole and diastole, and incremental stress $\Delta\sigma_\theta$ from diastole to systole in the red, blue, and green lines, respectively. Both the circumferential stresses σ_θ at systole and diastole have a minimum at $\theta = 0°$ and 180° and the maximum at $\theta = 90°$. The incremental stress $\Delta\sigma_\theta$ has a minimum value at $\theta = 90°$ and maximum values at $\theta = 0°$ and 180°. The θ dependence in these results is reasonable because the artery expands along the short-axis direction ($\theta = 0°$ and 180°) more than the long-axis direction ($\theta = 90°$) because of the deformation from the ellipse at diastole to the circular shape at systole.

Figure 6 shows the calculated results for the shape dependence of σ_θ. As the aspect ratio increased and the vessel cross-section collapsed, the circumferential stress σ_θ became larger at systole and smaller at diastole, resulting in a larger incremental stress $\Delta\sigma_\theta$. The larger the cross-sectional area of the vessel collapsed, the larger the maximum strain during one heartbeat; therefore, this calculation result is reasonable.

Figure 7 shows the calculation results for the pushing pressure p_3 dependence of σ_θ. As the pushing pressure p_3 increased, σ_θ decreased, while its incremental stress $\Delta\sigma_\theta$ was almost unchanged. The larger the pressure p_3, the greater the force in the direction in which the vessel wall elongated in the circumferential direction, and it caused greater stress in the compressive direction to balance it. On the other hand, $\Delta\sigma_\theta$ was almost constant when p_3 was constant during one heartbeat. Therefore, we considered that this is the reason why the elasticity has been stably estimated at rest in our previous study because the pushing pressure has been kept constant at rest.[30)]

4.2. Results of the in vivo experiments

Pushing pressures p_3 of 59.3 mmHg, 64.2 mmHg, and 81.1 mmHg were applied in the three measurements. The pushing pressure was almost constant during each measurement and was not affected by the heartbeats. Therefore, the assumption in Sect. 3.1 was confirmed as reasonable. The average of the pushing pressures measured by the four sensors was used to estimate the elastic moduli of the radial artery. Figure 8 shows the relationship between blood pressure and strain during one heartbeat between the succeeding R waves of the electrocardiogram for each pushing pressure p_3. The strain increased with an increase in p_3, which is consistent with the previous results obtained by our research group.[31)] From the dashed lines in Fig. 8 obtained by connecting the most distant points in the hysteresis loops, the elastic modulus E was estimated based on the proposed method. For the conventional method, the elastic modulus was estimated as the slope of the line; therefore, the elastic

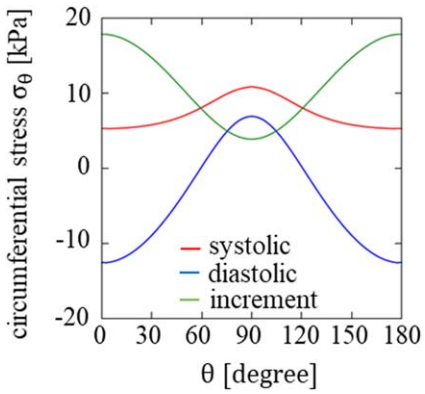

Fig. 5. (Color online) θ dependence of the circumferential stresses σ_θ for systole, diastole, and incremental stress.

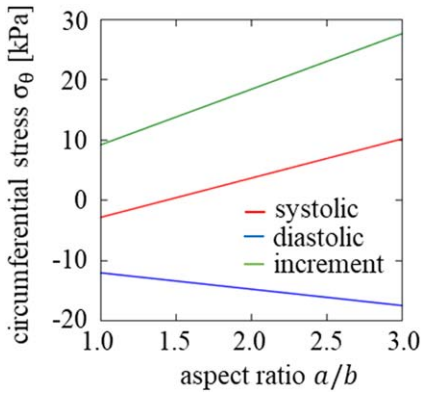

Fig. 6. (Color online) Dependence of the circumferential stresses σ_θ for systole, diastole, and incremental stress on the aspect ratio a/b of the cross-section of the vessel.

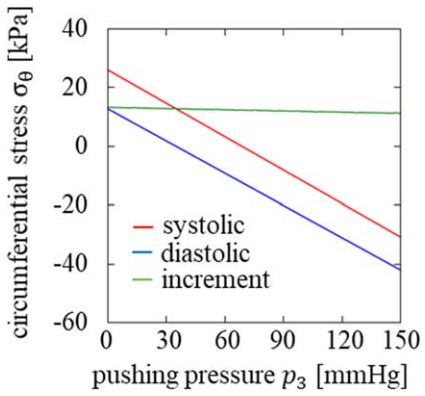

Fig. 7. (Color online) Dependence of the circumferential stresses σ_θ for systole, diastole, and incremental stress on pushing pressure p_3.

modulus estimated by the conventional method greatly varied depending on the pushing pressure p_3.

Figures 9(a–i)–9(c–ii) show the B-mode images of the radial artery for the three different pressures p_3. Figure 9(i) correspond to the diastole, and Fig. 9(ii) correspond to the systole. Figures 9(a)–9(c) show the results at $p_3 = 59.3$ mmHg, $p_3 = 64.2$ mmHg, and $p_3 = 81.1$ mmHg, respectively. Table I shows the measured values of the intravascular pressure p_1, the pushing pressure p_3, the long radius a and the short radius b of the vessel for each B-mode image. Ellipses determined by the obtained a and b values were superimposed on each B-mode image of Fig. 9. Each ellipse was well fitted,

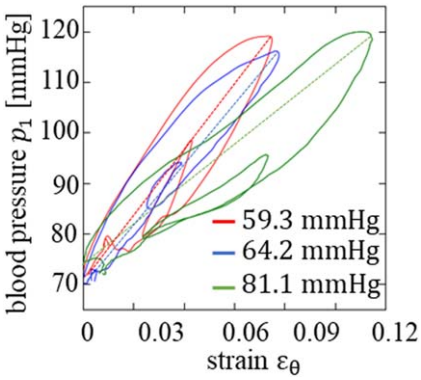

Fig. 8. (Color online) Relationships between the blood pressure and the strain of the radial artery with different pushing pressures p_3 of 59.3, 64.2, and 81.1 mmHg. The dashed lines connect the most distant points in the hysteresis loops.

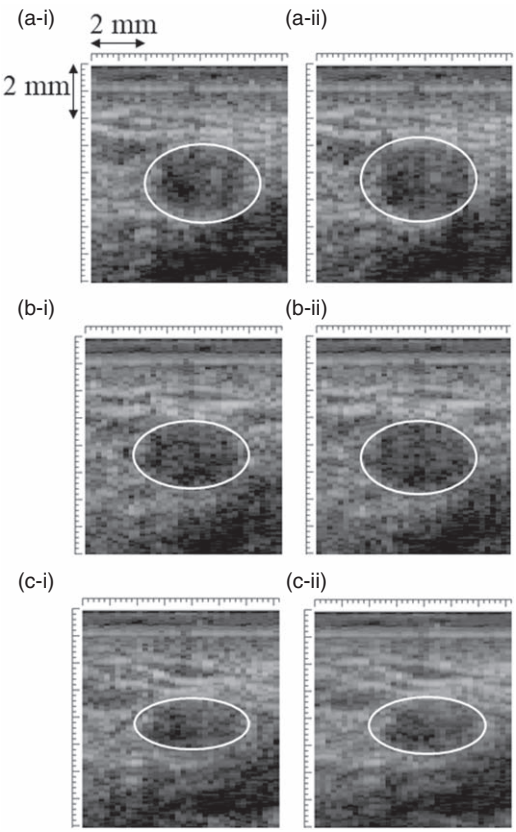

Fig. 9. B-mode images of the radial artery (i) at diastole and (ii) at systole: (a) $p_3 = 59.3$ mmHg, (b) $p_3 = 64.2$ mmHg, and (c) $p_3 = 81.1$ mmHg. Ellipses drawn based on the obtained a and b were superimposed on the vessel cross-section.

Table I. Measured results of each parameter for Figs. 9(a–i)–9(c–ii).

Data	p_1 [mmHg]	p_3 [mmHg]	a [mm]	b [mm]
9(a-i)	71.6	59.3	2.25	1.47
9(a-ii)	119.2	59.3	2.25	1.58
9(b-i)	72.1	64.2	2.25	1.25
9(b-ii)	120.0	64.2	2.25	1.13
9(c-i)	72.1	81.1	2.25	0.95
9(c-ii)	119.2	81.1	2.25	1.08

and the assumption of the cross-section of an ellipse was reasonable.

Figure 10 shows the relationships between the incremental strain $\Delta\varepsilon_\theta$ and the corresponding stress $3(\Delta\sigma_\theta - \Delta\sigma_r)/4$ of Eq. (9) for the three p_3. The stresses $3(\Delta\sigma_\theta - \Delta\sigma_r)/4$ estimated by the proposed method at the systole and diastole were plotted. It was confirmed that the slopes of the straight lines reflecting the elastic moduli were closer to each other than those by the conventional method shown in Fig. 8.

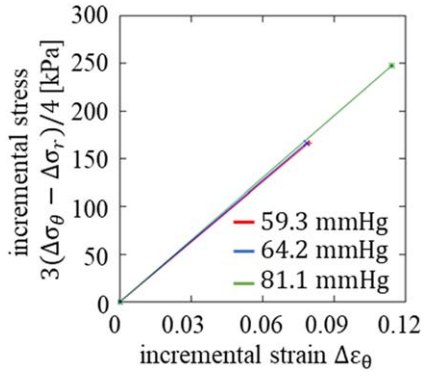

Fig. 10. (Color online) Relationships between the stress $3(\sigma_\theta - \sigma_r)/4$ and strain ε_θ for the proposed method for various values of p_3.

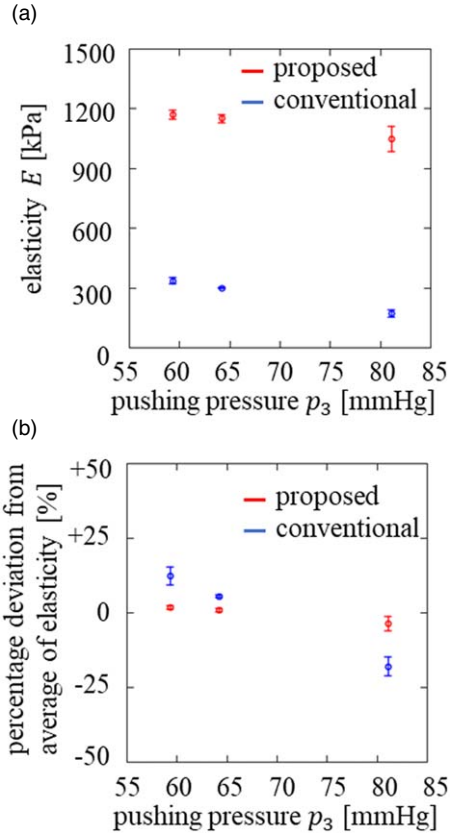

Fig. 11. (Color online) Elastic modulus values estimated by the proposed and conventional methods. (a) Absolute values and (b) percentage deviations from the average elasticity.

Figure 11(a) shows the relationship between the pushing pressure p_3 and the averages and standard deviations of the elastic moduli E estimated by the proposed and conventional methods. The elastic moduli estimated by the conventional method were small and significantly decreased as p_3 increased. Figure 11(b) shows the relationship between the pushing pressure p_3 and the percentage deviations from the averages of the estimated elastic moduli obtained by the proposed and conventional methods. The estimates of E by

the conventional method changed by –36% to +25% depending on p_3, while those by the proposed method changed by –7 to +3%. Therefore, the effect of the pushing pressure on the resulting change in the shape of the vessel was markedly reduced. In a previous study,[26] the decrease in elastic modulus during FMD was approximately 40%. Therefore, as the elastic modulus in the present study is considered to be accurate enough, the proposed method is suitable for evaluating the decrease in the elastic modulus during FMD.

Based on the known biomechanical attributes of the vessel wall,[37] it is expected that the measured elastic modulus increases as the initial stresses on the vessel wall σ_r and σ_θ increase. However, in the present study, the elastic moduli obtained by both the proposed and conventional methods were estimated to decrease with increasing pushing pressure, as shown in Fig. 11. The increase in pushing pressure caused the vessel to collapse, an increase in the incremental stress at the short axis of the vessel, as shown in Fig. 5, and an increase in the incremental stress, as shown in Fig. 6. These increased the change in the short vessel diameter by heartbeat and increased the strain by heartbeat. Moreover, the conventional method approximates the intravascular pressure as the stress on the vessel wall. This approximation causes a large dependence of the elastic modulus on the pushing pressure, as shown in Fig. 11. In the proposed method, the pressure dependence of the estimated elastic modulus was markedly decreased by calculating the stress while considering the changes in the vessel shape due to the pushing pressure applied by the ultrasound probe. In the present study, the shape of the vessel wall was assumed to be part of a circle in the calculation of the strain. However, because the actual shape of the vessel wall was an ellipse, as shown in Fig. 9, depending on the pushing pressure, the calculation of the strain might have affected the estimation of the elastic modulus. To solve this problem, it is necessary to further consider a strain calculation based on the actual shape of the vessel or to estimate the elastic modulus using Eq. (8) to measure the strain in the direction of the through-wall using an ultrasonic probe with a higher resolution.

As shown in Fig. 11, the elastic moduli E estimated by the proposed method are larger than those of the conventional method. The circumferential incremental stress $\Delta\sigma_\theta$ increased as the aspect ratio a/b increased, as shown in Fig. 6. The increase in stress due to the change in the cross-sectional shape of the vessel was not considered in the conventional method. As a result, $\Delta\sigma_\theta$ was estimated to be smaller, as shown in Fig. 11, and the elasticity by the conventional method was estimated to be smaller than the true elasticity obtained with Eq. (9). Therefore, the larger estimated values obtained using the proposed method are more reasonable.

5. Conclusions

In the present study, to accurately measure the elastic modulus of a deformed blood vessel, a series of equations were derived to estimate the elastic modulus by considering the pushing pressure applied by an ultrasound probe, which deforms the blood vessel. The derived equations were confirmed by changing the stresses through numerical simulations using parameters applied from actual measurements. Moreover, we compared the values estimated by the proposed method with those estimated using the conventional method in in vivo measurements for various pushing pressure values. The results revealed that the proposed method reduces the pressure dependence of the estimated elastic moduli. However, the proposed method cannot completely eliminate pressure dependence. Because the calculation of the strain is still insufficient, it is necessary to introduce the shape of the vessel into a strain calculation in future research. This method has the potential to measure elasticity more accurately than other methods and can be applied to the evaluation of endothelial function during the FMD reaction.

Acknowledgments

This work was partially supported by JSPS KAKENHI 20H02156.

ORCID iDs

Shohei Mori https://orcid.org/0000-0002-5494-1055
Mototaka Arakawa https://orcid.org/0000-0001-9386-645X
Hiroshi Kanai https://orcid.org/0000-0002-6567-1687

1) K. J. Foreman et al., Lancet **392**, 2052 (2018).
2) S. J. Nicholls et al., J Am Cardiol. **47**, 1967 (2006).
3) S. Motoyama et al., J. Am. Coll. Cardiol. **54**, 49 (2009).
4) D. A. McDonald and B. Flow, *in Arteries* (Edward Arnold, London, 1974) 2nd ed., p. 284.
5) J. I. Weitz, J. B. Chair, G. P. Clagett, M. E. Farkouh, J. M. Porter, D. L. Sackett, D. E. Strandness Jr, and L. M. Taylor, Circulation **94**, 3026 (1996).
6) K. Shirai, J. Utino, K. Otsuka, and M. Takata, J. Atheroscler. Thromb. **13**, 101 (2006).
7) K. Hayashi, H. Handa, S. Nagasawa, A. Okumura, and K. Moritake, J. Biomech. **13**, 175 (1980).
8) S. Akiyama, S. Mori, M. Arakawa, and H. Kanai, Jpn. J. Appl. Phys. **60**, SDDA07 (2021).
9) R. Ross, New Engl. J. Med. **340**, 115 (1999).
10) J. A. Panza, A. A. Quyyumi, J. E. Brush Jr, and S. E. Epstein, New Engl. J. Med. **323**, 22 (1990).
11) Y. Higashi, S. Sasaki, K. Nakagawa, H. Matsuura, T. Oshima, and K. Chayama, New Engl. J. Med. **346**, 1954 (2002).
12) M. C. Coretti et al., J. Am. Coll. Cardiol. **39**, 257 (2002).
13) N. M. AbdelMaboud and H. H. Elsaid, Egypt. J. Radiat. Nucl. Med. **44**, 237 (2013).
14) T. Nakamura et al., Int. J. Cardiol. **167**, 555 (2013).
15) E. J. Benjamin, M. G. Larson, M. J. Keyes, G. F. Mitchell, R. S. Vasan, J. F. Keaney Jr, B. T. Lehman, S. Fan, E. Osypiuk, and J. A. Vita, Circulation **109**, 613 (2004).
16) H. Tomiyama, C. Matsumoto, J. Yamada, T. Teramoto, K. Abe, H. Ohta, Y. Kiso, T. Kawauchi, and A. Yamashina, Hypertens Res. **31**, 2019 (2008).
17) I. B. Wilkinson et al., Arterioscler. Thrombosis Vascular Biol. **22**, 147 (2002).
18) S. Van. Doornum, G. McColl, A. Jenkins, D. J. Green, and I. P. Wicks, Arthritis Rheumatol. **48**, 72 (2003).
19) P. Hjemdahl and P. Friberg, J. Hypertens. **14**, 147 (1996).
20) H. Iwasaki, M. Shichiri, F. Marumo, and Y. Hirata, Endocrinology **142**, 564 (2001).
21) R. F. Furchgott, Circ. Res. **53**, 557 (1983).
22) K. Ikeshita, H. Hasegawa, and H. Kanai, Jpn. J. Appl. Phys. **47**, 4165 (2008).
23) K. Ikeshita, H. Hasegawa, and H. Kanai, Jpn. J. Appl. Phys. **48**, 07GJ10 (2009).
24) K. Ikeshita, H. Hasegawa, and H. Kanai, Jpn. J. Appl. Phys. **50**, 07HF08 (2011).
25) K. Ikeshita, H. Hasegawa, and H. Kanai, Jpn. J. Appl. Phys. **51**, 07GF14 (2012).

26) M. Sato, H. Hasegawa, and H. Kanai, Jpn. J. Appl. Phys. **53**, 07KF03 (2014).
27) Y. Sakai, H. Taki, and H. Kanai, Jpn. J. Appl. Phys. **55**, 07KF11 (2016).
28) M. Arakawa, K. Kudo, K. Kobayashi, and H. Kanai, Sens. Actuators A **286**, 146 (2019).
29) M. Arakawa, T. Saito, S. Mori, S. Ohba, K. Kobayashi, and H. Kanai, Sens. Actuators A **297**, 111487 (2019).
30) T. Saito, S. Mori, M. Arakawa, S. Ohba, K. Kobayashi, and H. Kanai, Jpn. J. Appl. Phys. **59**, SKKE04 (2020).
31) Y. Shoji, S. Mori, M. Arakawa, S. Ohba, K. Kobayashi, and H. Kanai, Proc. Int. Ultrason. Symp. 2020, p. 1.
32) Y. Shoji, S. Mori, M. Arakawa, S. Ohba, K. Kobayashi, and H. Kanai, Jpn. J. Appl. Phys. **60**, SDDE03 (2021).
33) Y. Shoji, M. Arakawa, S. Mori, S. Ohba, K. Kobayashi, and H. Kanai, Proc. Symp. Ultrason. Electr. 42, 2Pb5–10, 2021.
34) H. Hasegawa and H. Kanai, Proc. 2007 IEEE Int. Ultrasonics Symp. 2007, p. 860.
35) D. J. Patel, J. S. Janicki, and R. N. Vaishnav, Circ. Res. **32**, 93 (1973).
36) H. Kanai, M. Sato, Y. Koiwa, and N. Chubachi, IEEE Trans. Ultrason. Ferroelectr. Freq. Control **43**, 791 (1996).
37) P. B. Dobrin, Physiol. Rev. **58**, 397 (1978).